Anal. Chem. **2008,** *80,* 1918−1927

Improving the Efficiency of IMS−IMS by a Combing Technique

Samuel I. Merenbloom,[†] Stormy L. Koeniger,[†,#] Brian C. Bohrer,[†] Stephen J. Valentine,[‡] and David E. Clemmer*,[†]

Department of Chemistry, Indiana University, Bloomington, Indiana 47405, and Predictive Physiology and Medicine, Bloomington, Indiana 47403

A simple method for increasing the efficiency of multidimensional ion mobility spectrometry (IMS−IMS) measurements (as defined by the number of two-dimensional data sets necessary to sample all of the ions in a complex mixture) is illustrated. In this approach, components from a packet containing a mixture of ions are introduced into the first IMS drift region where they are separated based on differences in mobility. At the exit of this region, narrow distributions of ions having identical mobilities are selected, subjected to gentle activation conditions that are intended to induce conformational changes, and transmitted into a second IMS drift region where the new conformations are separated. Here, we describe a simple timing sequence associated with selection and activation of multiple distributions at the entrance of the second drift region in a systematic fashion that improves the efficiency of two-dimensional IMS−IMS by a factor of ∼8. The method is illustrated by examination of a mixture of tryptic peptides from human hemoglobin.

Recently, we described a two-dimensional ion mobility spectrometry technique (IMS−IMS),[1] whereby (1) a packet of ions is separated in the first drift tube, (2) ions of a specified mobility are selected by gating away all ions having different mobilities, (3) selected ions are collisionally activated, such that new structures may be formed, and (4) the new distribution of conformations is separated again in a second drift tube prior to analysis by mass spectrometry (MS). In favorable cases, the differences in structures between the distributions of initial (selected) states and states formed upon activation make it possible to resolve different components that would otherwise have identical mobilities. For mixtures of tryptic peptides, we demonstrated that the peak capacity of this type of IMS−IMS approach can be surprisingly high, exceeding 1000 prior to the MS analysis.[2]

A drawback of this method is that the experimental efficiency (as measured by the number of data sets necessary to sample all of the ions in a complex mixture) is low. The process of selecting a single narrow distribution of ions for activation and separation in the second drift tube inherently limits subsequent stages of analysis to only those ions selected. This inefficiency is analogous to that imposed by selection of specific mass-to-charge (m/z) ions for tandem mass spectrometry (MS/MS) studies.[3] In IMS−IMS studies, in order to examine the entire distribution of ions in a complex mixture, it is necessary to scan the selection gate time across the entire range of observed drift times; ideally, the selection gate duration should be similar to the diffusion-limited peak width[4] of a packet containing a single species as it reaches the selection region. For example, an instrument that is capable of generating a peak capacity of ∼100 in the first IMS separation would yield an optimal IMS−IMS experimental efficiency of ∼1% if one were to sample the ions as described above. Thus, although the peak capacity improvement is significant, the total time required to examine the entire distribution is ∼100 times longer than the time required for a one-dimensional IMS measurement.

Here, we describe a simple, multiplexing method for improving the efficiency of IMS−IMS. By utilizing the selection gate at intervals that are less than the total drift time through the entire instrument, it is possible to more efficiently use the original ion distribution. In this case, we select multiple packets of ions at the end of the first IMS region for activation and further separation. Because the change in drift time associated with the change in conformation is much less than the drift time through the entire instrument, it is possible to substantially improve the efficiency. The approach is demonstrated by examining a mixture of peptides obtained from enzymatic digestion of human hemoglobin where a factor of ∼8 improvement in experimental efficiency is obtained. This improvement is system- and instrument-dependent. Optimization will depend upon the magnitude of mobility shifts after activation (that are typical for the ions under investigation), as well as specifics associated with instrumental geometries. Both of these factors are discussed below. The present work is closely related to many other studies that aim to improve the efficiency

* To whom correspondence should be addressed. E-mail: clemmer@indiana.edu.

† Indiana University.

‡ Predictive Physiology and Medicine.

Present address: Abbott Laboratories, Abbott Park, IL 60064.

(1) Koeniger, S. L.; Merenbloom, S. I.; Valentine, S. J.; Udseth, H.; Smith, R.; Clemmer, D. E. *Anal. Chem.* **2006**, *78*, 4161−4174.

(2) Merenbloom, S. I.; Bohrer, B. C.; Koeniger, S. L.; Clemmer, D. E. *Anal. Chem.* **2007**, *79*, 515−522.

(3) (a) Wanless, G. G.; Glock, G. A., Jr. *Anal. Chem.* **1967**, *39*, 2. (b) McLafferty, F. W.; Bryce, T. A. *J. Chem. Soc., Chem. Commun.* **1967**, 1215.

(4) (a) Wannier, G. H. *Bell Syst. Tech. J.* **1953**, *32*, 170−254. (b) Revercomb, H. E.; Mason, E. A. *Anal. Chem.* **1975**, *47*, 970−983. (c) Mason, E. A.; McDaniel, E. W. *Transport Properties of Ions in Gases*; Wiley: New York, 1988.

10.1021/ac7018602 CCC: $40.75
Published on Web 02/22/2008

of complex mixture analysis, including combinations of liquid chromatographies with MS[5,6] and IMS-MS techniques,[7] gel-based methods,[8–11] and other techniques based on the mobilities of ions through gases (including a recent two-dimensional field asymmetric [(FA)IMS–IMS] approach).[12,13] Additionally, this work is related to studies aimed at improving the peak capacity of ion mobility separations[14] and the duty cycle of both IMS[15] and IMS-MS.[16]

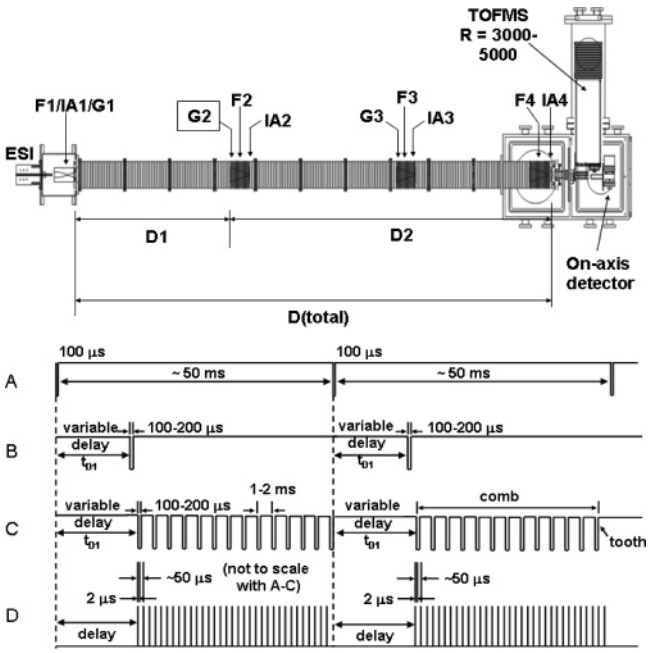

Figure 1. Schematic of IMS–IMS–IMS-TOF instrument. Ions are gated through G1 and then undergo mobility separation in D1. Ions can be selected based on mobility at G2 and G3; only G2 was employed in these studies and therefore is highlighted. The G1 pulse (A) initiates the mobility separation, and all other pulses are delayed with respect to it. If no pulse is applied to G2, all ions traverse the entire drift tube. Application of the pulse labeled B at G2 allows a narrow range of ions having a specified mobility into D2. This process can be multiplexed by using the pulse sequence labeled C; due to its appearance, we refer to this pulse sequence as a comb and the individual selections as teeth. Last, pulse sequence D is used to inject ions into the TOF mass analyzer. Collisional activation of mobility-selected ions is performed at the region labeled IA2, and ions can be fragmented at IA4 in a parallel fashion. Please note that the timing sequences are not drawn to scale.

EXPERIMENTAL SECTION

General Information. Figure 1 shows a schematic diagram of the instrument employed for these studies. General aspects of IMS theory and instrumentation are described elsewhere;[1,4,17–25] only a short description of key elements associated with multiplexing is provided here. Briefly, a continuous beam of ions produced

(5) (a) Link, A. J.; Eng, J.; Schieltz, D. M.; Carmack, E.; Mize, G. J.; Morris, D. R.; Garvik, B. M.; Yates, J. R. *Nat. Biotechnol.* **1999**, *17*, 676–682. (b) Wolters, D. A.; Washburn, M. P.; Yates, J. R. *Anal. Chem.* **2001**, *73*, 5683–5690. (c) Washburn, M. P.; Wolters, D.; Yates, J. R. *Nat. Biotechnol.* **2001**, *19*, 242–247. (d) Peng, J. M.; Schwartz, D.; Elias, J. E.; Thoreen, C. C.; Cheng, D. M.; Marsischky, G.; Roelofs, J.; Finley, D.; Gygi, S. P. *Nat. Biotechnol.* **2003**, *21*, 921–926. (e) Skop, A. R.; Liu, H.; Yates, J. R.; Meyer, B. J.; Heald, R. *Science* **2004**, *305*, 61–66.

(6) For descriptions of recent work involving multidimensional LC coupled with MS see the following reviews and references therein: (a) Nagele, E.; Vollmer, M.; Horth, P.; Vad, C. *Expert Rev. Proteomics* **2004**, *1* (1), 37–46. (b) Cooper, J. W.; Wang, Y. J.; Lee, C. S. *Electrophoresis* **2004**, *25*, 3913–3926.

(7) (a) Valentine, S. J.; Kulchania, M.; Srebalus Barnes, C. A.; Clemmer, D. E. *Int. J. Mass Spectrom.* **2001**, *212*, 97–109. (b) Matz, L. M.; Dion, H. M.; Hill, H. H. *J. Chromatogr., A* **2002**, *946*, 59–68. (c) Lee, Y. J.; Hoaglund-Hyzer, C. S.; Srebalus Barnes, C. A.; Hilderbrand, A. E.; Valentine, S. J.; Clemmer, D. E. *J. Chromatogr., B* **2002**, *782*, 343–351. (d) Myung, S.; Lee, Y. L.; Moon, M. H.; Taraszka, J. A.; Sowell, R. A.; Koeniger, S. L.; Hilderbrand A. E.; Valentine, S. J.; Cherbas, L.; Cherbas, P.; Kaufmann, T. C.; Miller, D. F.; Mechref, Y.; Novotny, M. V.; Ewing, M.; Clemmer D. E. *Anal. Chem.* **2003**, *75*, 5137–5145. (e) Moon, M. H.; Myung, S.; Plasencia, M.; Hilderbrand, A. E.; Clemmer, D. E. *J. Proteome Res.* **2003**, *2*, 589–597. (f) Sowell, R. A.; Koeniger, S. L.; Valentine, S. J.; Moon, M. H.; Clemmer, D. E. *J. Am. Soc. Mass Spectrom.* **2004**, *15*, 1341–1353. (g) Taraszka, J. A.; Kurulugama, R.; Sowell, R.; Valentine, S. J.; Koeniger, S. L; Arnold, R. J.; Miller, D. F.; Kaufman, T. C.; Clemmer, D. E. *J. Proteome Res.* **2005**, *4*, 1223–1237. (h) Taraszka, J. A.; Gao, X.; Valentine, S. J.; Sowell, R. A.; Koeniger, S. L; Miller, D. F.; Kaufman, T. C.; Clemmer, D. E. *J. Proteome Res.* **2005**, *4*, 1238–1247. (i) Koeniger, S. L.; Valentine, S. J.; Myung, S.; Plasencia, M.; Lee, Y. L.; Clemmer, D. E. *J. Proteome Res.* **2005**, *4*, 25–35. (j) Valentine, S. J.; Plasencia, M. D.; Liu, X.; Krishnan, M.; Naylor, S.; Udseth, H. R.; Smith, R. D.; Clemmer, D. E. *J. Proteome Res.* **2006**, *5*, 2977–2984. (k) Liu, X.; Valentine, S. J.; Plasencia, M. D.; Trimpin, S.; Naylor, S.; Clemmer, D. E. *J. Am. Soc. Mass Spectrom.* **2007**, *18*, 1249–1264.

(8) Shevchenko, A.; Jensen, O. N.; Podtelejnikov, A. V.; Sagliocco, F.; Wilm, M.; Vorm, O.; Mortensen, P.; Shevchenko, A.; Boucherie, H.; Mann, M. *Proc. Natl. Acad. Sci. U.S.A.* **1996**, *93*, 14440–14445.

(9) Gauss, C.; Kalkum, M.; Löwe, M.; Lehrach, H.; Klose, J. *Electrophoresis* **1999**, *20*, 575–600.

(10) Gygi, S. P.; Corthals, G. L.; Zhang, Y.; Rochon, Y.; Aebersold, R. *Proc. Natl. Acad. Sci. U.S.A.* **2000**, *97*, 9390–9395.

(11) (a) Rabilloud, T. *Proteomics* **2002**, *2*, 3–10. (b) Görg, A.; Weiss, W.; Dunn, M. J. *Proteomics* **2004**, *4*, 3665–3685.

(12) Tang, K.; Li, F.; Shvartsburg, A. A.; Stritmatter, E. F.; Smith, R. D. *Anal. Chem.* **2005**, *77*, 6381–6388.

(13) (a) Barnett, D. A.; Ells, B.; Guevremont, R.; Purves, R. W. *J. Am. Soc. Mass Spectrom.* **2002**, *13*, 1282–1291. (b) Kapron, J.; Mauriala, T.; Clark, P.; Purves, R. W.; Bateman, K. *Rapid Commun. Mass Spectrom.* **2006**, *20*, 1504–1510.

(14) (a) Asbury, G. R.; Hill, H. H. *Anal. Chem.* **2000**, *72*, 580–584. (b) Matz, L. M.; Hill, H. H.; Beegle, L. W.; Kanik, I. *J. Am. Soc. Mass Spectrom.* **2002**, *13*, 300–307. (c) Ruotolo, B. T.; Gillig, K. G.; Stone, E. G.; Russell, D. H. *J. Chromatogr., B* **2002**, *782*, 385–392. (d) Ruotolo, B. T.; McLean, J. A.; Gillig, K. J.; Russell, D. H. *J. Mass Spectrom.* **2004**, *39*, 361–367. (e) Ruotolo, B. T.; McLean, J. A.; Gillig, K. J.; Russell, D. H. *J. Am. Soc. Mass Spectrom.* **2005**, *16*, 158–165.

(15) (a) Knorr, F. J.; Eatherton, R. L.; Siems, W. F.; Hill, H. H. *Anal. Chem.* **1985**, *57*, 402–406. (b) St. Louis, R. H.; Siems, W. F.; Hill, H. H. *Anal. Chem.* **1992**, *64*, 171–177. (c) Chen, Y. H.; Siems, W. F.; Hill, H. H. *Anal. Chim. Acta* **1996**, *334*, 75–84. (d) Szumlas, A. W.; Hieftje, G. M. *Anal. Chim. Acta* **2006**, *566*, 45–54. (e) Clowers, B. H.; Siems, W. F.; Hill, H. H.; Massick, S. M. *Anal. Chem.* **2006**, *78*, 44–51. (f) Szumlas, A. W.; Ray, S. J.; Hieftje, G. M. *Anal. Chem.* **2006**, *78*, 4474–4481.

(16) Belov, M. E.; Buschbach, M. A.; Prior, D. C.; Tang, K.; Smith, R. D. *Anal. Chem.* **2007**, *79*, 2451–2462.

(17) (a) Clemmer, D. E.; Jarrold, M. F. *J. Mass Spectrom.* **1997**, *32*, 577–592. (b) Hoaglund-Hyzer, C. S.; Counterman, A. E.; Clemmer, D. E. *Chem. Rev.* **1999**, *99*, 3037–3079.

(18) (a) Mesleh, M. F.; Hunter, J. M.; Shvartsburg, A. A.; Schatz, G. C.; Jarrold, M. F. *J. Phys. Chem.* **1996**, *100*, 16082–16086. (b) Wyttenbach, T.; von Helden, G.; Batka, J. J., Jr.; Carlat, D.; Bowers, M. T. *J. Am. Soc. Mass Spectrom.* **1997**, *8*, 275. (c) Shvartsburg, A. A.; Jarrold, M. F. *Chem. Phys. Lett.* **1996**, *261*, 86–91. (d) Shvartsburg, A. A.; Hudgins, R. R.; Dugourd, P.; Jarrold, M. F. *Chem. Soc. Rev.* **2001**, *30*, 26–35.

(19) Cohen, M. J.; Karasek, F. W. *J. Chromatogr. Sci.* **1970**, *8*, 330.

(20) St. Louis, R. H.; Hill, H. H. *Crit. Rev. Anal. Chem.* **1990**, *21*, 321–355.

(21) Jarrold, M. F. *J. Phys. Chem.* **1995**, *99*, 11–21.

(22) (a) Wyttenbach, T.; von Helden, G.; Batka, J. J., Jr.; Carlat, D.; Bowers, M. T. *J. Am. Soc. Mass Spectrom.* **1996**, *8*, 275–282. (b) Wyttenbach, T.; Bowers, M. T. *Mod. Mass Spectrom. Top. Curr. Chem.* **2003**, *225*, 207–232.

(23) Creaser, C. S.; Benyezzar, M.; Griffiths, J. R.; Stygall, J. W. *Anal. Chem.* **2000**, *72*, 2724–2729.

(24) Collins, D. C.; Lee, M. L. *Anal. Bioanal. Chem.* **2002**, *372*, 66–73.

(25) Tang, K.; Shvartsburg, A. A.; Lee, H.; Prior, D. C.; Buschbach, M. A.; Li, F.; Tomachev, A.; Anderson, G. A.; Smith, R. D. *Anal. Chem.* **2005**, *77*, 3330–3339.

by electrospray ionization (ESI)[26] is focused into and accumulated in a Smith-geometry ion funnel (F1).[27] Short (100 μs) pulses of ions are released into the drift tube (D1) via an electrostatic gate (G1). The drift tube can be operated at buffer gas pressures of 2.50−3.50 Torr; for these experiments, it was operated at 3.16 Torr. For studies in which cross section information is to be obtained, pure He buffer gas is used; in these experiments, however, 1% N_2 was added to the system, to facilitate higher voltages for the fragmentation of ions at the exit of the drift tube.[28] As ions travel through the buffer gas, different species separate due to differences in their mobilities.[4,17] Immediately following D1 are a second ion gate (G2) and ion funnel (F2), followed by an activation region (IA2). This combination of elements allows mobility-selected ions to be focused in the off-axis dimensions and collisionally activated prior to the second mobility separation. A third gate (G3) and funnel (F3) set can be operated in a similar fashion. However, in these studies F3 has been fixed to transmit all ions. Finally, a funnel (F4) at the back of the drift tube is used to focus ions into an ion activation region (IA4). The field in IA4 can be modulated between conditions that favor transmission of precursor ions and those that induce ion fragmentation as described previously.[28,29] The length of the entire drift tube is ~290 cm; D1 is 95.1 cm. All drift regions are operated using a drift field of 9.0 V cm^{-1}; each ion funnel region is operated at 11.0 V cm^{-1}. Under these conditions, rf fields in the ion funnels usually range from 110 to 250 V_{p-p}, at frequencies of 220−440 kHz.

Ion Gating for Multiplexing IMS−IMS Experiments. Figure 1 also shows typical pulse sequences used in these experiments (and those that lead to improvements in efficiency). As noted, experiments are initiated by the G1 pulse (sequence A in Figure 1), and for convenience, all other pulses associated with gating (sequences B and C in Figure 1) and timing for MS data collection (sequence D in Figure 1) are referenced with respect to this pulse. The improvement in efficiency is associated with the number of pulses applied to G2 between subsequent G1 pulses (sequences B and C in Figure 1). For example, if two pulses are used in sequence C, the efficiency is doubled. A 10-fold advantage would be obtained by using 10 pulses.

In order to sample the entire distribution of ions, the delay of pulse sequence C is systematically varied. For example, if 100 μs duration pulses at a spacing between pulses of 500 μs are utilized, then five consecutive experiments in which the initial delay (associated with the first gating pulse) is increased by 100 μs between each experiment would adequately cover the entire distribution of ions. We provide an illustration of this below. Because of the appearance of the pulses in sequence C, as well as the systematic way that the pulse sequence is shifted in order to cover the entire distribution, we refer to this approach as "combing". With this analogy, each of the pulses in sequence C is called a tooth in a specific comb and the shift of the entire sequence C represents a comb through the data.

MS Analysis. Ions exit the drift tube and are focused into a time-of-flight mass spectrometer (TOF-MS) for detection.[30] In early work, we referred to the IMS-MS measurement as a "nested" measurement because flight times are much shorter than drift times and can be recorded within individual drift time windows.[30] As such, the smallest increment that drift times can be measured in corresponds to the maximum flight time recorded by the TOF-MS (in these experiments, 975 windows of ~65 μs each). This remains the case in these studies, and because flight-time measurements are synchronized with respect to G1 (as before), no changes to the acquisition system are required. Experimental conditions can be controlled such that the reproducibility of drift time measurements is high (to within 1−2 drift windows, or <1% of the drift times examined in these studies). The resolving power of the mass spectrometer used in this instrument is typically on the order of 3000−5000.

Ion Activation at IA2 and IA4. The instrument used for these studies includes four ion activation regions (IA1 through 4, Figure 1). Only IA2 and IA4 are used here. IA2, a region defined by the last two lenses of the ion funnel (an rf-free region), is 0.3 cm long and used to gently activate ions in order to cause structural changes between the D1 and D2 regions. Under the buffer gas conditions employed, slight structural changes (i.e., changes in drift times greater than 1%) of mobility-selected peptide ions appear when a bias of as little as 5 V is applied across the IA2 region. In the discussion given below, we refer to activation in which no dissociation occurs as collisional activation (CA). At a bias of 80 V, structural changes are observed across a wide range of mobilities, for both peptide and protein ions. Biases in excess of 80 V are used to induce structural changes in larger peptides and proteins; however, slight fragmentation of smaller, higher mobility peptides is observed. When a bias of more than ~150 V is used, both peptide and protein ions undergo substantial collisional heating and fragment ions are formed.[31] Below, we refer to this process as collision-induced dissociation (CID). In the following studies, a bias of 70 V was applied across the IA2 region, to ensure minimal CID within the drift tube.

The IA4 region is analogous in design to the split-field drift tube explained previously.[28] By increasing the voltage difference between the conical lens and beryllium−copper (BeCu) plate at the exit of the drift tube, it is possible to generate fragment ions from the mobility-separated ions.[29] In this configuration fragment ions that are formed have drift times that are defined by the precursor ions from which they are generated. In the case of two-dimensional IMS−IMS, these drift times may be a composite of multiple precursor ion states. This was originally described as a "parallel" CID method, because unlike MS/MS there is no initial selection and thus an advantage in efficiency;[29] however, it is important to note that, technically, ions are separated in space and time (e.g., one could also refer to the approach as a high-

(26) Fenn, J. B.; Mann, M.; Meng, C. K.; Wong, S. F.; Whitehouse, C. M. *Science* **1989**, *246*, 64−71.

(27) (a) Shaffer, S. A.; Tang, K. Q.; Anderson, G. A.; Prior, D. C.; Udseth, H. R.; Smith, R. D. *Rapid Commun. Mass Spectrom.* **1997**, *11*, 1813−1817. (b) Shaffer, S. A.; Prior, D. C.; Anderson, G. A.; Udseth, H. R.; Smith, R. D. *Anal. Chem.* **1998**, *70*, 4111−4119. (c) Shaffer, S. A.; Tolmachev, A.; Prior, D. C.; Anderson, G. A.; Udseth, H. R.; Smith, R. D. *Anal. Chem.* **1999**, *71*, 2957−2964. (d) Kim, T.; Tolmachev, A. V.; Harkewicz, R.; Prior, D. C.; Anderson, G.; Udseth, H. R.; Smith, R. D.; Bailey, T. H.; Rakov, S.; Futrell, J. H. *Anal. Chem.* **2000**, *72*, 2247−2255.

(28) Valentine, S. J.; Koeniger, S. L.; Clemmer, D. E. *Anal. Chem.* **2003**, *75*, 6202−6208.

(29) Hoaglund-Hyzer, C. S.; Li, J.; Clemmer, D. E. *Anal. Chem.* **2000**, *72*, 2737−2740.

(30) (a) Hoaglund, C. S.; Valentine, S. J.; Sporleder, C. R.; Reilly, J. P.; Clemmer, D. E. *Anal. Chem.* **1998**, *70*, 2236−2242. (b) Srebalus, C. A.; Li, J.; Marshall, W. S.; Clemmer, D. E. *Anal. Chem.* **1999**, *71*, 3918−3927.

(31) Merenbloom, S. I.; Koeniger, S. L.; Valentine, S. J.; Plasencia, M. D.; Clemmer, D. E. *Anal. Chem.* **2006**, *78*, 2802−2809.

speed serial approach). We prefer the original nomenclature and use it below.

Sample Preparation and Electrospray Source Conditions. Tryptic peptides from human hemoglobin (Sigma, St. Louis, MO, 90% purity) were produced by enzymatic digestion as described previously.[2,7] Solutions (0.25 mg mL^{-1} peptides in water/acetonitrile/acetic acid, 49:49:2% by volume) were infused directly into a pulled capillary tip at a flow rate of 0.25 μL min^{-1}, controlled by a syringe pump (kd Scientific, Holliston, MA). A 2.0 kV bias was applied to the tip by use of a platinum electrode for ESI.

RESULTS AND DISCUSSION

Illustration of Multiplexing for IMS−IMS with a Hypothetical Data Set and Factors Affecting the Multiplex Advantage. It is useful to begin by illustrating this approach conceptually. Figure 2 shows plots associated with a hypothetical analysis of a complex mixture. In this case, the mixture complexity exceeds the experimental peak capacity such that a broad feature is observed across the drift time distribution associated with all ions (Figure 2a). Selection of a single feature from the mobility distribution (Figure 2b, as denoted by the bold dotted line) results in the transmission of a single peak, which may or may not contain several species; in this example, it contains three. The goal of the combing analysis is to increase the throughput and efficiency of the IMS−IMS measurement, while at the same time create regions where ions may be resolved; selection of ions at three specific times (noted by dotted lines) by transmission through the G2 gate without activation (thus assuming no change in mobility) would lead to three sharp peaks, as shown (Figure 2c). Note that the dotted lines reflect the arrival times of the ions after traveling through the entire drift assembly in Figure 1; because the G2 gate in these experiments occurs approximately one-third of the way through the instrument, selection of ions at this point corresponds to one-third of their total drift times. In this hypothetical system, each selection contains three types of ions, which, upon activation, may change conformation and shift into unoccupied regions of the spectrum (Figure 2d). Note that the spacing between selections is such that there is no overlap between ions upon activation.

In the above example, three selections were made across the distribution of ions, resulting in a 3-fold gain in throughput compared to a single IMS−IMS selection. If 10 selections were made, this advantage would become 10-fold, but with a loss of resolving power for the second drift dimension. As the spacing between adjacent teeth decreases, ions that change significantly in mobility upon activation will begin to overlap with species selected in adjacent teeth. Ultimately, gains in efficiency and peak capacity are limited by how much the mobilities of ions change upon activation. Prior work involving a range of other systems, including clusters,[32,33] larger proteins,[32,34] other types of biomolecules,[35] and synthetic polymers,[36] shows that changes in mobility are system-dependent. For the gently activated peptide ions (doubly and triply protonated ions having m/z values of ~500−1500) prior work suggests that the change in mobilities can be as large as 11%.[2] Additionally, the magnitude of change is dependent on the ion selected, with more change expected for large, multiply charged species than for smaller, less charged ones.

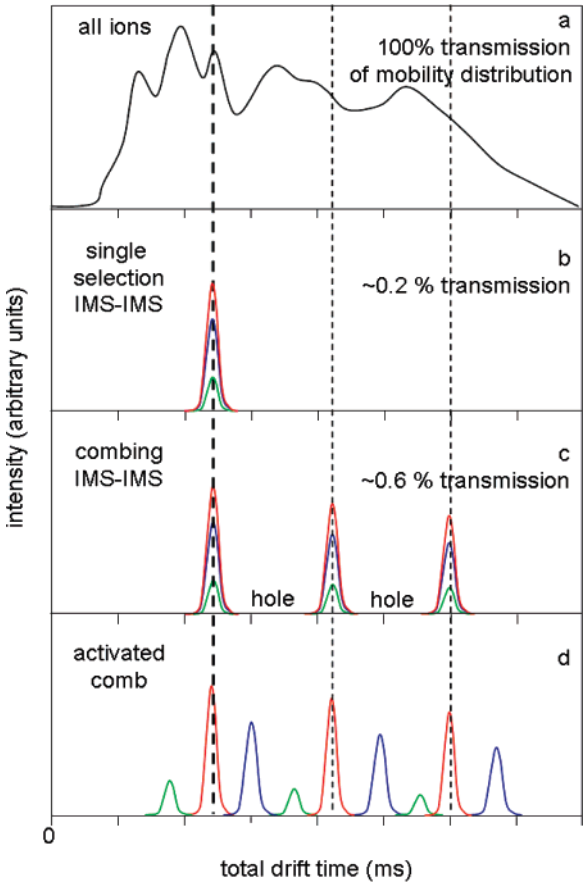

Figure 2. Top plot (a) shows a hypothetical ion mobility distribution for a complex mixture of ions obtained by allowing all ions to traverse the entire drift tube. Mobility selection of a narrow distribution of ions at G2 results in the transmission of a single peak corresponding to a small percentage of the total ion current (b, see text for details). Applying a combing pulse centered about the times highlighted to G2 results in the transmission of three packets of ions, each containing three different species; without collisional activation, all ions retain their original mobilities and therefore experience no change in drift time (middle plot, c). Collisional activation of the selected ions in IA2 may lead to structural changes in some of the ion populations and therefore shifts in mobility. In each packet of ions, the green ions adopt a higher mobility structure, while the blue ions adopt a lower mobility structure; the red ions undergo no change in mobility. Because empty areas between peaks (holes) were created by the initial selections, the activated ions now have regions of drift space in which to resolve from one another (bottom plot, d).

From this type of consideration (as well as considerations of the instrument geometry and complexity of the sample to be analyzed) one can determine a reasonable spacing (one that enhances the efficiency without giving up too much of the advantages associated with increased peak capacity). For these experiments, tooth spacing was determined by the largest change in drift time anticipated for the lowest mobility ion. As an example,

(32) Clemmer, D. E.; Jarrold, M. F. *J. Mass Spectrom.* **1997**, *32*, 577−592.
(33) (a) Von Helden, G.; Hsu, M. T.; Gotts, N.; Bowers, M. T. *J. Phys. Chem.* **1993**, *97*, 8182−8192. (b) Jarrold, M. F. *J. Phys. Chem.* **1995**, *99*, 11−21. (c) Hunter, J. M.; Jarrold, M. F. *J. Am. Chem. Soc.* **1995**, *117*, 10317−10324. (d) Counterman, A. E.; Clemmer, D. E. *J. Phys. Chem. B* **2001**, *105*, 8092−8096. (e) Julian, R. R.; Hodyss, R.; Kinnear, B.; Jarrold, M. F.; Beauchamp, J. L. *J. Phys. Chem. B* **2002**, *106*, 1219−1228. (f) Myung, S.; Julian, R. R.; Nantia, S. C.; Cooks, R. G.; Clemmer, D. E. *J. Phys. Chem. B* **2004**, *108*, 6105−6111. (g) Julian, R. R.; Myung, S.; Clemmer, D. E. *J. Phys. Chem. B* **2005**, *109*, 440−444. (h) Myung, S.; Fioroni, M.; Julian, R. R.;

for an ion with a drift time of 50 ms, a 5% change in mobility would result in a change of drift time of ±2.5 ms. Twice this amount would be how far apart teeth should be separated as they exit the drift tube to ensure no overlap of ions upon activation; again, because the selection gate occurs at some fraction of the length of the entire drift tube, it is approximately at this fraction of the spacing that teeth should be spaced for their application at the gate. It is possible to confirm the initial selection time of the final activated peak by finding the same m/z value in a related data set that utilizes no activation between the drift regions.

Multiplex Advantage Considerations in Terms of Observed Ion Current. The efficiency gains of the combing technique can also be observed in the higher ion currents measured for an individual combing experiment compared to an individual IMS−IMS-MS experiment. For ESI of biomolecular samples, several measurements show that incoming ion currents are typically on the order of 1−20 nA.[27,37] Although simulations show that ion funnels are capable of handling incoming currents of this magnitude with little to no loss in transmission,[37] experimental parameters (field, pressure, rf frequency/amplitude) limit the actual transmission to ∼30−50% of this value.[27] However, nearly all of the lost current is attributed to solvent ions of little analytical relevance that are either too small or too large to be adequately focused by the rf fields; therefore, transmission for ions of interest approaches 100%, with some m/z bias observed.[27] Because transmission into the drift tube is dependent on the parameters and geometry of the source ion funnel, for these considerations, a transmitted current of 1 nA through F1 (in nontrapping mode) is assumed.

Once the voltage on G1 is raised and an IMS experiment is initiated, the current observed at the detector is a function of both the IMS duty cycle and the trapping efficiency of the ion funnel F1. If F1 were to have no trapping efficiency, i.e., the G1 voltage merely blocks the incoming ion beam during the course of an IMS experiment, the percentage of the incoming ion current exiting the F1 region will be exactly equal to the IMS duty cycle. For example, a 100 μs wide pulse every 65 ms would produce an ion current entering the drift tube of $(0.100/65.100 \times 1\ \text{nA}) = 0.0015$ nA, or 1.5 pA. Assuming the space charge limit of the funnel is not reached in the fill time, the current observed for a funnel of appreciable trapping efficiency is equal to the percentage of charges trapped in the fill time divided by the length of the drift separation. For these experiments the fill time was equal to the duration of the drift experiment (the beam was continually filling the ion funnel); therefore, the current exiting the funnel was equal to the trapping efficiency multiplied by the incoming current; a trapping efficiency of 20% would yield an outgoing current of 0.20 nA, or 200 pA. These ions would then separate through the drift tube based on their differences in mobilities, such that the observed current in any one TOF experiment varies on the basis of the most abundant mobilities. However, the overall amount of ions reaching the TOF source will be this value, minus any losses to diffusion, grids, or conductance-limiting orifices, which will be addressed below.

Although the ion funnels F2, F3, and F4 are situated such that there are no losses due to diffusion across the range of mobilities studied here, as mentioned in detail elsewhere,[1] 90% transmittance grid is used at the exit of F1 (to trap ions), at the entrances and exits of F2, F3, and F4 (to keep the rf fields from impinging upon the drift regions), as well as at G2 and G3 (for a total of nine grids). For an instrument containing n elements of transmittance t, the observed intensity I will be $I = I_o t^n$, where I_o is the intensity prior to entering the instrument. Therefore, $(90\%)^9 = 39\%$ of the ions exiting F1 will reach the exit of the drift tube, decreasing the 200 pA exiting F1 to 78 pA exiting the drift tube.

For IMS-MS, the observed ion current would be dependent on any losses in the ion optics prior to the TOF-MS source as well as the TOF duty cycle. A recently published ion funnel trap oa-TOF instrument reported transmission efficiencies of ∼35% from the exit of the ion funnel to a charge collector located immediately after the TOF source; this was attributed primarily to losses at conductance-limiting orifices as well as the radial expansion of the ion cloud as it exits the ion funnel.[38] Although the ion optics region of our instrument is not as long as that cited, losses due to these factors should be comparable, such that ∼40% of ions transmitted through the drift tube (∼31 pA) reach the TOF source. For a TOF-MS admitting a 2 μs wide pulse of ions every 70 μs, that becomes 0.87 pA $(2/72 \times 31)$ of observed current in the duration of one IMS-MS experiment. This corresponds to the "100% transmission of mobility distribution" shown in Figure 2a.

In IMS−IMS, a narrow selection containing ions of a specified mobility is taken from the distribution of ions. For these particular experiments, a 120 μs wide selection was made from the 65 ms wide all-ion distribution; if we assume that the signal is evenly spread across this distribution, then $(0.120/65.00 \times 100) = 0.185\%$ of the IMS-MS signal is observed; this is shown in Figure 2b. As mentioned above, the distribution of signal across drift times is mobility- and sample-dependent; this percentage can be higher or lower than that stated. By making several selections at the G2 gate, a gain in signal roughly equal to the number of selections

Koeniger, S. L.; Baik, M.-H.; Clemmer, D. E. *J. Am. Chem. Soc.* **2006**, *128*, 10833−10839. (i) Myung, S.; Lorton, P.; Merenbloom, S. I.; Fioroni, M.; Koeniger, S. L.; Julian, R. R.; Baik, M.-H.; Clemmer, D. E. *J. Am. Chem. Soc.* **2006**, *128*, 15988−15989.

(34) (a) Shelimov, K. B.; Jarrold, M. F. *J. Am. Chem. Soc.* **1997**, *119*, 2987−2994. (b) Hudgins, R. R.; Woenckhaus, J.; Jarrold, M. F. *Int. J. Mass Spectrom.* **1997**, *165*, 497−507. (c) Valentine, S. J.; Clemmer, D. E. *J. Am. Chem. Soc.* **1997**, *119*, 3558−3566. (d) Valentine, S. J.; Anderson, J. G.; Ellington, A. D.; Clemmer, D. E. *J. Phys. Chem. B* **1997**, *101*, 3891−3900. (e) Valentine, S. J.; Counterman, A. E.; Clemmer, D. E. *J. Am. Soc. Mass Spectrom.* **1997**, *8*, 954−961. (f) Li, J.; Taraszka, J. A.; Counterman, A. E.; Clemmer, D. E. *Int. J. Mass. Spectrom.* **1999**, *185/186/187*, 37−47. (g) Purves R. W.; Barnett, D. A.; Guevremont, R. *Int. J. Mass Spectrom.* **2000**, *197*, 163−177. (h) Robinson, E. W.; Williams, E. R. *J. Am. Soc. Mass Spectrom.* **2005**, *16*, 1427−1437.

(35) For IMS of nucleic acids/oligonucleotides: (a) Hoaglund, C. S.; Liu, Y.; Ellington, A. D.; Pagel, M.; Clemmer, D. E. *J. Am. Chem. Soc.* **1997**, *119*, 9051−9052. (b) Koomen, J. M.; Ruotolo, B. T.; Gillig, K. J.; McLean, J. A.; Russell, D. H.; Kang, M. J.; Dunbar, K. R.; Fuhrer, K.; Gonin, M.; Schultz, J. A. *Anal. Bioanal. Chem.* **2002**, *373*, 612−617. For IMS of oligosaccharides: (c) Liu, Y.; Clemmer, D. E. *Anal. Chem.* **1997**, *69*, 2504−2509. (d) Lee, S.; Wyttenbach, T.; Bowers, M. T. *Int. J. Mass Spectrom.* **1997**, *167*, 605−614. (e) Gabryelski, W.; Froese, K. L. *J. Am. Soc. Mass Spectrom.* **2003**, *14*, 265−277. (f) Clowers, B. H.; Dwivedi, P.; Steiner, W. E.; Hill, H. H.; Bendiak, B. *J. Am. Soc. Mass Spectrom.* **2005**, *16*, 660−669.

(36) (a) Von Helden, G.; Wyttenbach, T.; Bowers, M. T. *Science* **1995**, *267*, 1483−1485. (b) Wyttenbach, T.; Helden, G.; Bowers, M. T. *Int. J. Mass Spectrom. Ion Processes* **1995**, *146*, 349−364. (c) Gidden, J.; Wyttenbach, T.; Jackson, A. T.; Scrivens, J. H.; Bowers, M. T. *J. Am. Chem. Soc.* **2000**, *122*, 4692−4699. (d) Trimpin, S.; Plasencia, M.; Isailovic, D.; Clemmer, D. E. *Anal. Chem.* **2007**, *79*, 7965−7974.

(37) Tolmachev, A. V.; Kim, T.; Udseth, H. R.; Smith, R. D.; Bailey, T. H.; Futrell, J. H. *Int. J. Mass Spectrom.* **2000**, *203*, 31−47.

(38) Ibrahim, Y.; Belov, M. E.; Tolmachev, A. V.; Prior, D. C.; Smith, R. D. *Anal. Chem.* **2007**, *79*, 7845−7852.

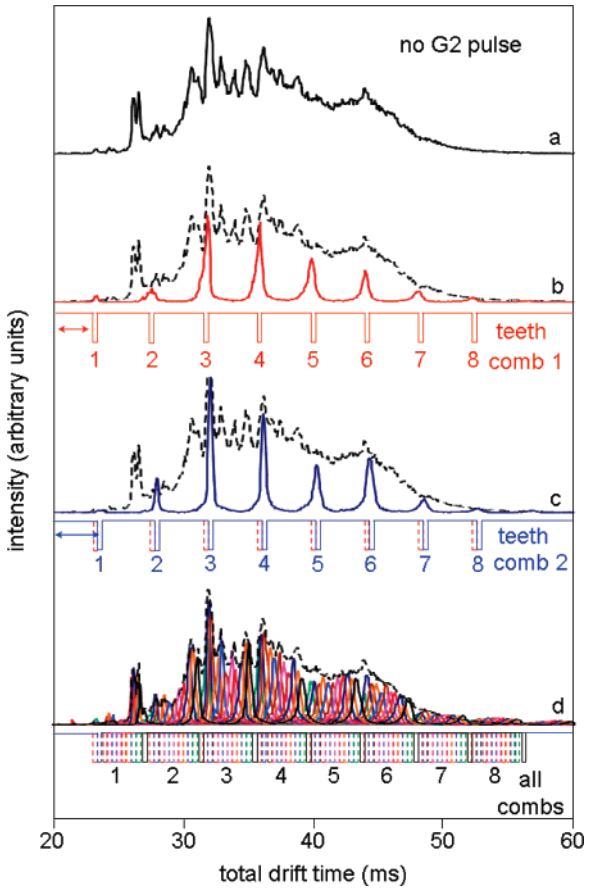

Figure 3. Ion mobility distributions for the tryptic digest of human hemoglobin, demonstrating combing IMS. The all-ion drift distribution is shown in (a). Application of the first comb (red pulse sequence) results in several equally spaced peaks, with empty regions in between (b). Increase of the initial delay time by the width of one tooth (advancing to the blue pulse sequence) results in the sampling of new ions (c, blue distribution); repeating this process until all combs are sampled results in the sampling of all ions and the replication of the original drift distribution (d).

made is observed. This is shown in Figure 2c; application of a combing pulse containing three teeth results in the transmission of three narrow peaks and approximately 3 times the signal in the combing experiment compared to the IMS−IMS experiment in Figure 2b. This gain in signal is also directly proportional to the gain in efficiency observed with combing IMS−IMS; it will now take 3 times fewer IMS−IMS experiments to sample all ions.

Examination of an IMS−IMS Separation of a Mixture of Tryptic Peptides with Multiplexing and Combing. Figure 3 shows examples of the IMS−IMS distributions that are obtained for a mixture of peptide ions from the tryptic digestion of human hemoglobin. When all ions are allowed to pass through the G2 region, a broad distribution of unresolved features that span drift times from ~22 to 55 ms is observed (Figure 3a). This is effectively the time required for these ions to travel through all drift regions and would correspond to a one-dimensional IMS experiment. Activation of G2, positioned at a distance that is approximately one-third of the total drift length, leads to transmission of only ions at specific times (roughly one-third the total drift time) in order to create pulses for the second IMS experiment. The result of transmitting eight 120 μs wide pulses through the G2 region at delay times of 7.657, 9.187, 10.717, 12.247, 13.777, 15.307, 16.837, and 18.367 ms (a spacing of 1.530 ms between pulses) is shown in Figure 3b.

As ions travel through the rest of the instrument, the ion packets (associated with each tooth pulse) diffuse to give peaks. In some cases, even without activation ions may shift to slightly shorter or longer times. Such shifts can arise if an ion is selected on the leading or tailing edge of its distribution. In such cases, the selected ion traverses the second IMS separation with the average mobility of the all-ion distribution. In this case, the change in mobility is small; for example, an ion with a drift time of 20 ms that has a full width at half-maximum peak width at the exit of the drift tube of 200 μs will experience a shift of less than 1% (~100 μs) if the leading or tailing edge has been selected. Additionally, any change in conformation (that occurs without activation) will influence the total drift times of the distributions. Generally, these types of shifts are much smaller than the shifts observed when substantial conformation changes are induced by activation.

By increasing the initial delay time by the G2 pulse width it is possible to generate a new comb. An example of this is shown in Figure 3c. In this case, each of the peaks observed corresponds to a slightly different distribution of ions with marginally lower mobilities (compared with the first comb). By sequentially increasing the delay in increments of the G2 pulse width, it is possible to sample the entire distribution of ions (an example showing 11 combs, each containing 8 teeth, is shown in Figure 3d).

The improvement in efficiency is measured by comparing the number of two-dimensional experiments necessary to sample the entire distribution of ions. In this particular example, the entire distribution is sampled with 11 individual combing experiments; to replicate this with conventional IMS−IMS using the single 120 μs pulse to cover the entire region would require 88 experiments. Thus, this sequence provides a factor of 8 (88/11) enhancement in experimental efficiency. For the system studied, this gain in efficiency is nearly the highest achievable (for this particular IMS-TOF instrumental geometry) without significant loss of peak capacity in the two-dimensional separation due to overlap of ions between adjacent teeth upon collisional activation.

Figure 4 shows another representation of this approach for the same human hemoglobin tryptic peptides. In Figure 4a, the distribution is plotted as a two-dimensional IMS-MS spectrum from drift times of 20−55 ms and an m/z range of 200−1200 showing most of the peaks that are present in the spectrum. Of the peaks that are observed, it is possible to assign 31 peaks to 23 different tryptic peptides based on comparisons of m/z values to anticipated tryptic peptides of both chains of human hemoglobin.[39] (If only the MS data are used, we assign only 22 of the peaks.) These assignments are summarized in Table 1.

The intense features in the IMS-MS data primarily correspond to $[M + 2H]^{2+}$ and higher charge-state peptides. This is advantageous as the larger, highly charged ions usually undergo more dramatic changes in conformation upon gentle activation at IA2. Figure 4b shows a single selection of ions at a G2 delay time of 9.601 ms (with no activation at IA2). The selection shows that it is possible to isolate a relatively small number of ions from the larger mixture. We note that Figure 4b shows a circle around the

(39) Anticipated tryptic peptides and fragments have been obtained (using monoisotopic masses) from the program ms-product. http://prospector.ucsf.edu/ucsfhtml4.0/msprod.htm.

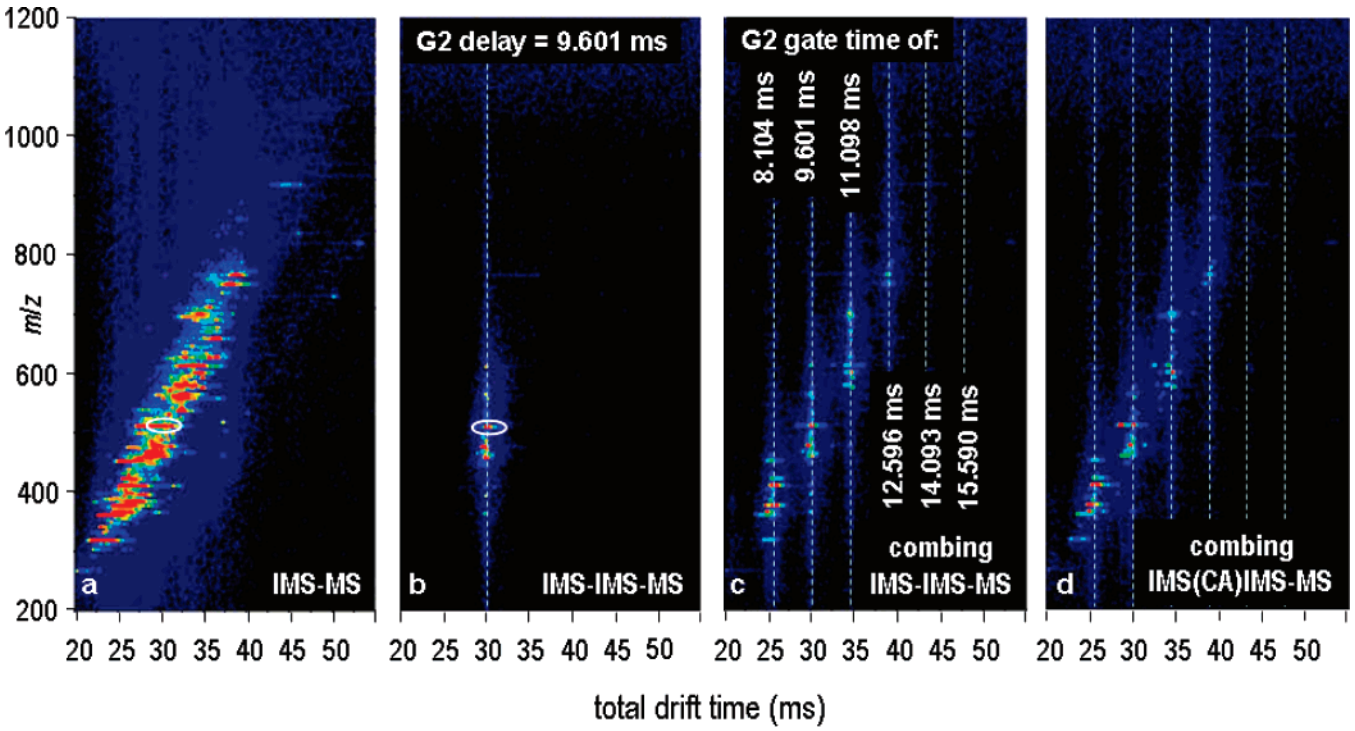

Figure 4. Nested drift (flight) distribution for electrosprayed human hemoglobin tryptic peptides obtained by allowing all ions to traverse the drift tube is shown in (a). The ion circled is the $[V_{18}-R_{32} + 3H]^{3+}$ ion at $t_D(m/z)$ 30.34(510.67), the focus of much of the discussion in the text. Performing a single mobility selection at G2 (9.601 ms delay time) of ions centered about 30.08 ms (shown by the dotted line) produces the nested drift (flight) distribution in (b). Plot c shows the spectrum obtained upon application of a combing pulse containing the 9.601 ms selection to G2; multiplexing the selection process has no effect on the nested measurement. Activation of the mobility-selected ions (IA2 = 70 V) produces plot d. The activated ions might experience structural changes and therefore can arrive at different drift times than expected based on their time of selection (shown by the dotted lines).

peak at $t_D(m/z) = 30.34(510.67)$, which is assigned to the $[V_{18}-R_{32} + 3H]^{3+}$ ion. We come back to this portion of the spectrum below in order to show the shift observed upon activation. Figure 4c illustrates the ability to multiplex selections and record IMS-MS data. Here, the combing pulse includes the 9.601 ms selection time (as well as selection times of 8.104, 11.098, 12.596, 14.093, and 15.590 ms). Clearly, this application can be done without influencing the MS measurement.

Upon increasing the potential across IA2 to 70 V, conditions where we gently activate the ions without measurable dissociation, we generate the corresponding IMS−IMS-MS spectrum shown in Figure 4d. This gentle activation allows the peptides to sample (and in favorable cases adopt) structures with different mobilities. The dashed lines that are shown indicate the original positions of the selected ions without any change in mobility after the combing region. From Figure 4d many ions appear to shift. Although these shifts appear small, the summation of them across the entire data set (all 11 activated combs) leads us to assign four additional peptide ions that were not resolved without activation. This is shown in Table 1. Although one advantage of IMS (and IMS−IMS) is the ability to separate ions of similar m/z due to their differences in mobilities, it can be seen that none of the additional ions observed in the activated combs overlap in m/z with any of the already observed peptides. The reason these peptides are assigned from the combing data is that they are observed free of overlapping spectral noise that hindered their detection in the IMS-MS data set. This is an illustration of one of the advantages associated with increased capacity.

It is important to consider the physical origin of the observed peak shifts. We have done this in detail for two tryptic peptides

Table 1. Summary of Observed Peptides[a]

		peptide	
m/z obsd	m/z calcd[b]	sequence[c]	chain[d]
365.29	365.21	$[V_2-K_8 + 2H]^{2+}$	(α)
376.13	376.19	$[L_{97}-R_{105} + 3H]^{3+}$	(β)
383.81	383.90	$[V_{134}-K_{145} + 3H]^{3+}$	(β)
409.71	409.72	$[V_{94}-K_{100} + 2H]^{2+}$	(α)
459.30	459.23	$[T_{42}-K_{57} + 4H]^{4+}$	(α)
466.81	466.76	$[S_{10}-K_{18} + 2H]^{2+}$	(β)
476.86	476.75	$[V_2-K_9 + 2H]^{2+}$	(β)
510.67	510.58	$[V_{18}-R_{32} + 3H]^{3+}$	(α)
536.34	536.28	$[M_{33}-K_{41} + 2H]^{2+}$	(α)
557.39	557.30	$[V_{68}-K_{83} + 3H]^{3+}$	(β)
563.84	563.79	$[L_{97}-R_{105} + 2H]^{2+}$	(β)
575.49	575.23	$[V_{134}-K_{145} + 2K]^{2+}$	(β)
612.07	611.97	$[T_{42}-K_{57} + 3H]^{3+}$	(α)
626.89	626.86	$[F_{129}-K_{140} + 2H]^{2+}$	(α)
658.04	657.84	$[V_{19}-R_{31} + 2H]^{2+}$	(β)
743.22	743.39	$[S_{10}-R_{31} + 3H]^{3+}$	(β)
750.06	749.88	$[V_{63}-K_{91} + 4H]^{4+}$	(α)
765.58	765.37	$[V_{18}-R_{32} + 2H]^{2+}$	(α)
835.59	835.45	$[V_{68}-K_{83} + 2H]^{2+}$	(β)
917.44	917.45	$[T_{42}-K_{57} + 2H]^{2+}$	(α)
999.69	999.50	$[V_{63}-K_{91} + 3H]^{3+}$	(α)
1029.92	1029.98	$[F_{42}-K_{60} + 2H]^{2+}$	(β)
524.52	524.63	$[F_{129}-R_{142} + 3H]^{3+}$	(α)
544.45	544.32	$[L_{92}-K_{100} + 2H]^{2+}$	(α)
600.12	600.00	$[K_{67}-K_{83} + 3H]^{3+}$	(β)
632.94	633.06	$[G_{84}-R_{105} + 4H]^{4+}$	(β)
690.10	689.85	$[E_{122}-K_{133} + 2H]^{2+}$	(β)
711.39	711.34	$[G_{84}-K_{96} + 2H]^{2+}$	(β)
857.50	857.46	$[V_{19}-R_{41} + 3H]^{3+}$	(β)
937.25	937.16	$[E_{122}-H_{147} + 3H]^{3+}$	(β)
989.91	989.88	$[L_{101}-K_{128} + 3H]^{3+}$	(α)
500.13	500.02	$[M_1-K_{18} + 4H]^{4+}$	(β)
849.18	849.20	$[K_{62}-R_{93} + 4H]^{4+}$	(α)
860.65	860.49	$[L_{106}-R_{121} + 2H]^{2+}$	(β)
871.64	871.72	$[S_{10}-R_{41} + 4H]^{4+}$	(β)

[a] The first 22 features were observed from the integrated mass spectrum alone. The middle nine were gained upon observation of the IMS-MS data set, whereas the final four were gained upon observation of all activated comb positions. [b] Calculated m/z values have been obtained (using monoisotopic masses) from the program ms-product at http://prospector.ucsf.edu/ucsfhtml4.0/msprod.htm. [c] Peptide sequence listed as N-terminal residue to C-terminal residue, along with position within the sequence of the protein. [d] α- or β-chain of human hemoglobin, respectively.

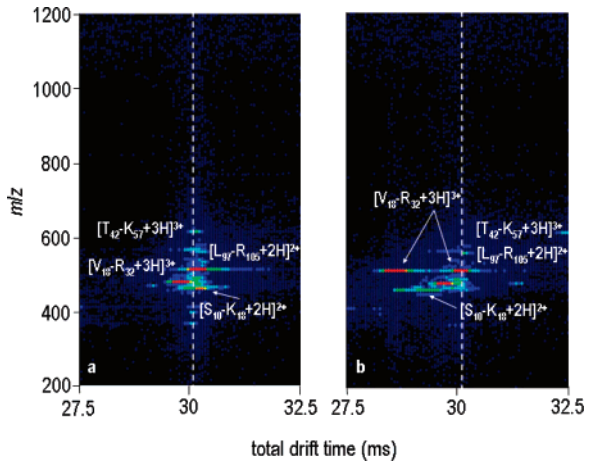

Figure 5. Expanded view of the nested drift (flight) distributions shown in Figure 4 (plots c and d), highlighting the 9.601 ms tooth of the comb. Plot a shows the distribution with no collisional activation at IA2; little deviation in drift times from the time expected based on the selection (30.08 ms, highlighted by the dotted white line) is observed. The plot labeled b is obtained when 70 V is applied to IA2, demonstrating the amount of shift observed upon gentle activation. The peptide sequence is listed as N-terminal residue to C-terminal residue, along with the position within the sequence of the protein.

of human hemoglobin using molecular modeling[2] and so only provide a brief description here. Those ions that adopt a more elongated structures shift to longer total drift times, while those ions becoming more compact shift toward shorter drift times. An important idea in these data is that these shift into regions of empty space between teeth (created by the selection process). In general, the physical origin of those ions that shift can be understood as an annealing process in the IA2 region. Those that shift apparently find a lower energy configuration upon activation. Those ions that do not shift may or may not be the same starting conformation. That is, the selected ion was already in its lowest energy conformation, or it assumed a lower energy conformation of a cross section indistinguishable from the initial state. A final explanation is that no shift is observed because there is no favored state. In this case, we anticipate that rapid mixing of conformations (on timescales that are shorter than the measurement) would lead us to observe a single sharp peak that would not be influenced by activation. Without prior knowledge of the peptide's conformational energy landscape, it is unknown whether a change will occur or not; however, experimental evidence shows that slight changes are common for many of the peptides studied.

Figure 5 shows a more detailed view of the data in Figure 4 (regions c and d in Figure 4). Over the range that is shown, these data in Figure 5a are effectively equivalent to those shown in Figure 4b, obtained using a single selection. Upon activation of 70 V at IA2, several ions undergo structural changes and resolve from the average mobility corresponding to the G2 selection time of 9.601 ms (30.08 ms is expected if we sampled a peak at its maximum and no change in mobility occurred). The $[T_{42}-K_{57}+3H]^{3+}$ ion, originally at $t_D(m/z)$ 30.15(612.07), elongates to a structure with a considerably lower mobility, arriving at a drift time of 32.43 ms. Interestingly, there is a population of this ion in the 11.098 ms tooth as well (Figure 4, parts c and d); its lack of significant structural change, coupled with the disappearance of the population in the 9.601 ms tooth, leads us to believe that the peak at 32.43 ms is from elongation of ions in the 9.601 ms tooth. The $[L_{97}-R_{105}+2H]^{2+}$ ion at $t_D(m/z)$ 30.22(563.84) stays relatively unchanged, whereas the $[S_{10}-K_{18}+2H]^{2+}$ ion [selected $t_D(m/z)$ 30.28(466.81)] adopts a more compact structure, with a final drift time of 28.71 ms.

In the initial data set we highlighted the peak at $t_D(m/z)$ 30.34-(510.67) by circling it. That peak corresponds to the $[V_{18}-R_{32}+$

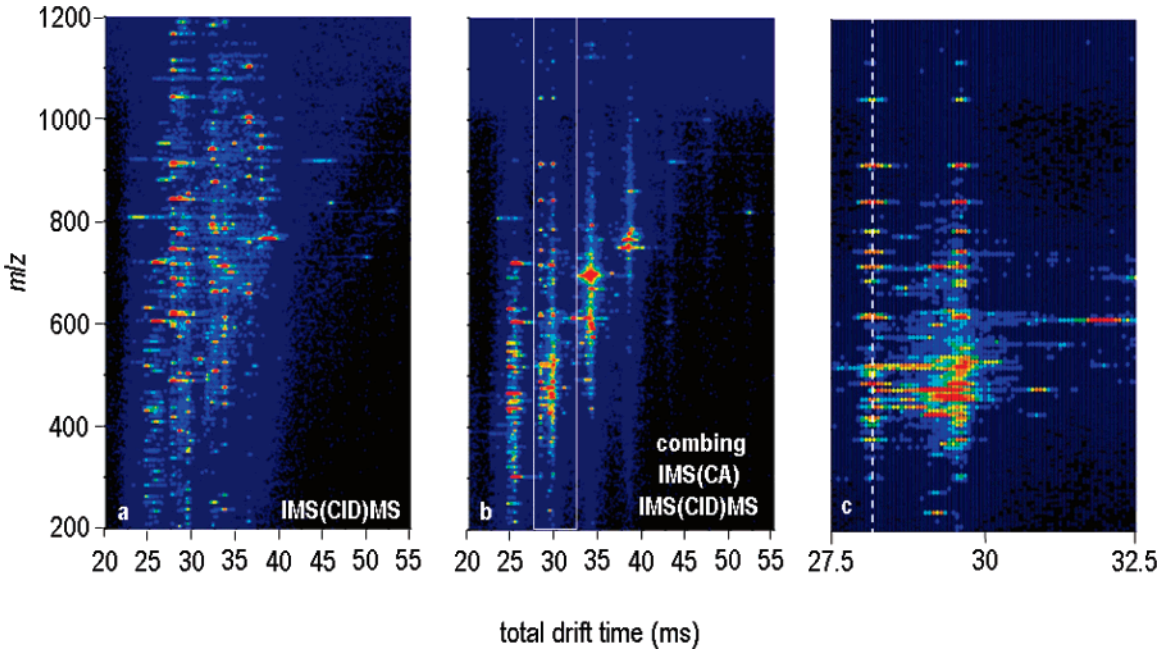

Figure 6. Nested drift (flight) distributions for the parallel CID of tryptic peptides of human hemoglobin. Fragmentation of ions with no pulse applied to G2 produces plot a. Fragmentation of the activated comb containing G2 selection times of 8.104, 9.601, 11.098, 12.596, 14.093, and 15.590 ms, respectively, is shown in (b). The white box in (b) denotes the region examined in greater detail in (c), highlighting the fragmentation of the mobility-resolved $[V_{18}-R_{32}+3H]^{3+}$ ion (dotted line). Integration of *m*/*z* values along the dotted line in (c) yields the mass spectrum in Figure 7d.

3H]$^{3+}$ ion. Prior to activation, this distribution shifts to slightly longer drift times than expected from the 9.601 ms G2 selection time. Upon activation, the peak splits into two resolvable peaks. One is still centered at 30.34 ms, while the other peak appears at 28.59 ms, indicating a higher mobility ion is favored after activation. We will focus more on this ion in the following section.

Illustration of a Multiplexed IMS(CA)−IMS(CID)-MS Data Set. The multiplexing and combing approaches can also be utilized with CID at the exit region of the drift tube. As described previously,[28,29] the ability to dissociate after separation offers a number of unique advantages, including the ability to examine dissociation patterns for different isomers (that may coexist in a mixture) as well as advantages associated with grouping fragment and precursor ions for interpretation. That is, all precursor ions are subjected to energizing collisions; fragments can be assigned to their respective precursors because of the coincidence in their drift times. Although the drift separation allows many precursors to be aligned with fragments, often this approach is still limited by the ability to initially resolve the precursors by IMS prior to fragmentation (i.e., the overlap of multiple precursors at the same drift time).

Combining IMS(CA)−IMS with combing allows parallel dissociation to be carried out on species that can be more highly resolved. Collisionally activated ions may move into the empty spaces between the comb teeth and be resolved prior to dissociation. A comparison of IMS(CID)-MS and IMS(CA)−IMS(CID)-MS for the same sample is provided in Figure 6. Figure 6a shows IMS(CID)-MS data for all of the ions that were separated based on a single IMS separation in Figure 4a. Although many ions are resolved, many still overlap. Figure 6b shows that the IMS(CA)−IMS(CID)-MS data set obtained for a pulse sequence corresponding to a single comb is substantially simplified. This is because the combing process eliminates signal across 10/11 of the spectrum prior to CA. Upon activation, ions may shift into empty regions before they reach the exit of the drift tube and are subjected to CID and MS analysis.

The advantages associated with creating the empty space and subsequent activation via this combing IMS(CA)−IMS process can be observed by examining a narrow drift region of Figure 6b in more detail; an expanded view of the 27.5−32.5 ms range (corresponding to a single tooth of the comb) is shown as Figure 6c. In this case, a range of different fragment ions are observed in this region. Most overlap and would not be resolved by IMS alone. The two most intense fragmentation spectra are observed at drift times of ~28 and 29.5 ms. Both of these fragmentation patterns correspond to fragments formed from the $[V_{18}-R_{32}+3H]^{3+}$ ion. Since no other precursor ions are observed at 28 ms in the IMS(CA)−IMS-MS parent distribution (Figure 5), we expect the fragments observed at this time to correspond to only those for this ion.

It is instructive to examine some mass spectral slices of the data in Figures 5 and 6. Integration of m/z values along a narrow region of drift times corresponding to the $[V_{18}-R_{32}+3H]^{3+}$ ion in Figure 5a produces the mass spectrum shown in Figure 7a. Peaks corresponding to tryptic peptides of human hemoglobin (allowing up to two missed cleavages) are labeled. Additionally, the inset highlights the region of the mass spectrum spanning values of m/z 550−650, showing several peptides within the tooth

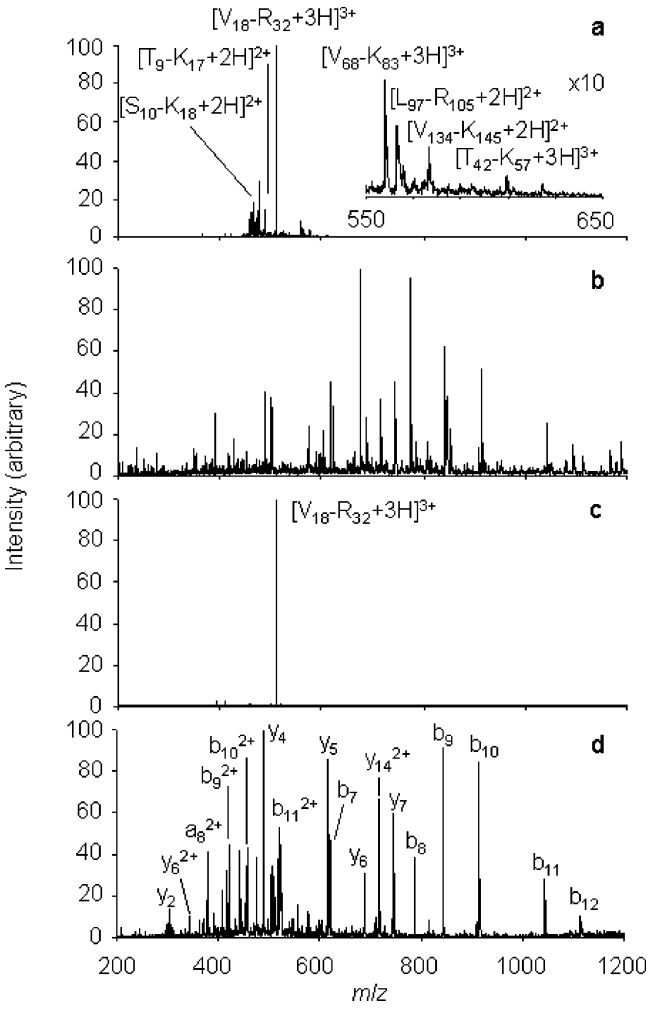

Figure 7. Mass spectra obtained by integrating *m*/*z* values across narrow regions of drift times corresponding to features of the $[V_{18}-R_{32}+3H]^{3+}$ ion. The top spectrum (a) comes from the data in Figure 5a, highlighting the amount of overlap observed among ions within the tooth. Plot b shows the fragmentation of these ions at IA4. Plot c is from the data in Figure 5b, demonstrating the resolution of the high mobility feature of the $[V_{18}-R_{32}+3H]^{3+}$ ion from the rest of the ions in the tooth. The fragmentation of this mobility-resolved ion at IA4 is shown in plot d.

having intensities too low to appear on the two-dimensional plot. This mass spectrum illustrates that there are a large number of ions present in a narrow region of drift space when no collisional activation is used; when the mixture of unresolved ions is exposed to energizing collisions at the exit of the drift tube the fragmentation pattern that is obtained (Figure 7b) is for a mixture of ions. The appearance of the spectrum in Figure 7b is similar to that obtained over the $[V_{18}-R_{32}+3H]^{3+}$ ion region with no combing. Overall, the overlap of multiple unresolved precursors and fragments complicates assignment of a fragment peak to the $[V_{18}-R_{32}+3H]^{3+}$ ion.

Alternatively, as mentioned above, the IMS(CA)−IMS spectrum (Figure 5b) shows that the $[V_{18}-R_{32}+3H]^{3+}$ ion adopts a structure with a higher mobility and the peak associated with this ion appears in a region of the spectrum that is relatively free of signals from other peptides. Figure 7c shows the mass spectrum obtained from IMS(CA)−IMS-MS analysis with no CID at the exit of the drift tube. The spectrum is dominated by a single peak at

$m/z = 510.67$, corresponding to the $[V_{18}-R_{32} + 3H]^{3+}$ ion. When the voltage at the exit of the drift tube is increased, the CID spectra described in Figure 6b is generated. The integrated mass spectrum obtained for the isolated ion is plotted as a mass spectrum in Figure 7d. Remarkably, all of the 34 features observed with an intensity of at least 10% of the base peak correspond to anticipated fragments (a-, b-, or y-type, or internal fragments).[39]

Finally, we point out that fragmentation of the mobility-resolved $[T_{42}-K_{57} + 3H]^{3+}$ ion at $t_D(m/z)$ 32.43(612.07) is obtained in parallel in this distribution, but not shown in the mass spectra of Figure 7. Moreover, in other regions where fragments are found to overlap in the IMS(CA)−IMS(CID)-MS data set, interpretation is greatly simplified relative to IMS(CID)-MS alone.

SUMMARY AND CONCLUSIONS

A new method for improving the throughput of a two-dimensional IMS−IMS analysis of complex mixtures has been presented. The approach provides a means of using a greater fraction of the ions separated in the first IMS region and is accomplished by allowing multiple packets of equal width and spacing of ions of specified mobilities from the first IMS separation to pass through the gating region into the second IMS region. In subsequent experiments the multiple gates are then systematically positioned such that it is possible to obtain two-dimensional information across the entire ion distribution. Examining a mixture of peptides from the tryptic digestion of human hemoglobin, we demonstrate an ~8-fold improvement in the two-dimensional sampling of the ions (as measured by the number of data sets necessary to sample all ions using the new pulse sequence compared to the single selection IMS−IMS method) with little loss in separation capacity. The greater peak capacity of this two-dimensional approach improves our ability to interpret fragmentation spectra, via creation of regions of mobility space with less overlap between ions. Further experiments are underway to develop optimal two-dimensional analyses for other types of systems.

ACKNOWLEDGMENT

This work is supported by Grants from the National Institutes of Health (AG-024547-02 and P41-RR018942) and funds from the MetaCyt initiative. One of the authors (S.I.M.) acknowledges the ACS Division of Analytical Chemistry and GlaxoSmithKline. In the interest of full disclosure, one of the authors from Indiana University (D.E.C.) is also a founder of PPM.

Received for review September 4, 2007. Accepted January 9, 2008.

AC7018602